

# MagneComm: Magnetometer-based Near-Field Communication

Hao Pan

Shanghai Jiao Tong University  
panh09@sjtu.edu.cn

Guangtao Xue

Shanghai Jiao Tong University  
gt\_xue@sjtu.edu.cn

Yi-Chao Chen

Shanghai Jiao Tong University  
yichao@utexas.edu

Xiaoyu Ji

Zhejiang University  
xji@zju.edu.cn

## ABSTRACT

Near-field communication (NFC) plays a crucial role in the operation of mobile devices to enhance applications such as payment, social networks, private communication, gaming, and etc. Despite of the convenience, existing NFC standards like ISO-13157 require additional hardware (*e.g.*, loop antenna and dedicated chip) and thereby hindering their wide-scale applications. In this work, we seek to propose a novel near-field communication protocol, MagneComm, which utilizes Magnetic Induction (MI) signals emitted from CPUs and captured by magnetometers on mobile devices for communication. Since CPUs and magnetometers are readily available components in mobile devices, MagneComm eliminates the requirement for special hardware and complements existing near-field communication protocols by providing additional bandwidth. We systematically analyze the characteristics of magnetic signals of CPUs and facilitate MagneComm with one-way communication, full-duplex communication, and multi-transmitter schemes in accordance with the hardware availability on devices. We prototype MagneComm on both laptops and smartphones. Extensive evaluation results show that MagneComm achieves up to 110 *bps* within 10 *cm*.

## CCS CONCEPTS

• **Human-centered computing** → **Mobile computing; Ubiquitous and mobile computing systems and tools**; • **Security and privacy** → *Mobile and wireless security*;

## KEYWORDS

near-field communication; magnetic induction; full-duplex

## 1 INTRODUCTION

Near-field communication (NFC) has been attracting considerable attention in recent years as it is facilitating a wide range of applications, including mobile payment, social networks, interactive gaming and etc. Nowadays, even the NFC module is integrated on major-brand smartphones, there is still a large portion of them without NFC due to the stringent requirement of NFC chips. Current NFC implementation is based on the ISO-13157 [19] standard which requires dedicated hardware, *i.e.* the NFC chip module consisting of an antenna and electric circuits for coding and decoding. The need for NFC chip, however, incurs extra costs and enlarges volume to size-limited smartphones and therefore greatly limits the applicability of NFC. On the other hand, even for NFC-capable devices, the NFC function is sometimes limited, *e.g.*, NFC on iPhones only supports Apple Pay.

A number of alternative methods have been devised to alleviate the pain brought by the standard NFC implementation. Typical examples are Bluetooth, acoustic [15, 27], visible light [17, 21, 25] and etc. Most of these approaches rely on commodity hardware or built-in sensors. Among them, Bluetooth is a popular technique and applied for short-range communication on mobile devices. However, existing alternative implementations of NFC also face problems. First, they are vulnerable to security issues. For example, Bluetooth works in a relatively longer communication range than the standard NFC and it is easy for attackers to eavesdrop the transmitted information. Second, the communication channels endure noise and interference, *e.g.*, Bluetooth is easily interfered with WiFi signals, not to mention the acoustic and the visible-light approaches. Therefore, existing alternative NFC implementations fail to satisfy both the security and performance requirements.

In this paper, we try to provide an NFC implementation scheme without dedicated hardware while keeping the security and performance concerns in mind. We adopt Magnetic Induction (MI) signal emitted from mobile devices as a communication channel and exploit the build-in magnetometer for signal reception. Specifically, we elaborately control the CPU module for transmission of MI signals, and the magnetometers equipped on commodity mobile devices for signal decoding. By carefully regulating the MI signals emitted from CPUs, and sensing it with the magnetometers on devices, two devices are able to communicate in a near-field manner. We develop this concept into a full-duplex communication system (referred to as MagneComm) using techniques such as pulse width and

---

Permission to make digital or hard copies of all or part of this work for personal or classroom use is granted without fee provided that copies are not made or distributed for profit or commercial advantage and that copies bear this notice and the full citation on the first page. Copyrights for components of this work owned by others than ACM must be honored. Abstracting with credit is permitted. To copy otherwise, or republish, to post on servers or to redistribute to lists, requires prior specific permission and / or a fee. Request permissions from [permissions@acm.org](mailto:permissions@acm.org).

*MobiCom '17, October 16–20, 2017, Snowbird, UT, USA*

© 2017 Association for Computing Machinery.

ACM ISBN 978-1-4503-4916-1/17/10...\$15.00

<https://doi.org/10.1145/3117811.3117824>

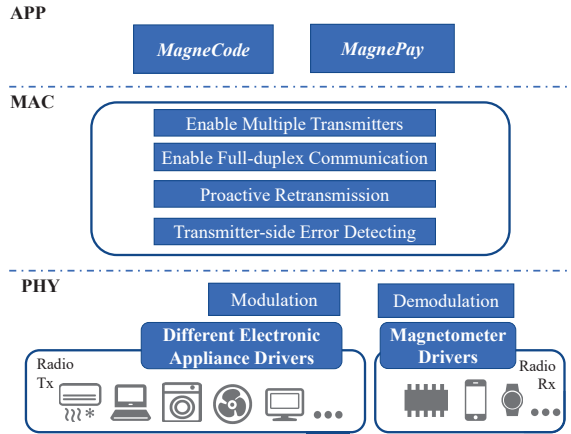


Figure 1: MagneComm Architecture.

amplitude modulation, channel estimation, proactive retransmission, and self-signal cancellation. The overall architecture of MagneComm is shown in Fig. 1 from a layered perspective.

The design of MagneComm poses a number of difficult challenges. First, precise control over CPU by job scheduling in operation systems (OS) to generate suitable MI signals is complicated. With this constraint, complex modulation schemes, such as OFDM (orthogonal frequency division multiplexing) are essentially infeasible. We first investigate the characteristics of MI signals from extensive experiments and finally combine the pulse width with amplitude modulation as the fundamental modulation scheme to strike a balance between transmission speed and accuracy. Second, concurrent running jobs on CPUs bring about interference during the transmission process, and thus increase confusion when detecting CPU’s MI signals. To guarantee the quality of transmission in noisy environments, we design a preamble for signal detection and a retransmission scheme. The retransmission scheme monitors the real-time CPU usage and the bit error distribution, and retransmits the previous corrupted packet if necessary. Third, to overcome the low sampling rate of the magnetometers on mobile devices, we adopt multiple transmitters in order to improve the transmission rate. We also exploit signal cancellation technique and design a subtraction algorithm to realize full-duplex communication, when both the two devices are equipped with magnetometers.

We implement the MagneComm prototype and evaluate the communication between laptops and smartphones, as well as between two laptops. The coded MI signals can be successfully captured and decoded by the magnetometers on smartphones and laptops. When MagneComm is applied between two laptops, a self-signal cancellation algorithm is applied at the terminal of the transmitter to counterbalance MI signals from its own CPU, thereby enabling dual-duplex communication. In our experiments, MagneComm is able to achieve throughput of up to 110 *bps* in average between two laptops, 12 *bps* between a laptop and a smartphone. Our prototype supports an operating range of up to 10 centimeters between devices.

MagneComm can flourish abundant applications. For example, the designed MagneCode built upon MagneComm

can enable an extended screen to obtain more information on mobile devices. The details of applications and their implementations are discussed in Sec. 7. The main contribution of this work can be summarized as follows:

- We propose *MagneComm*, a novel implementation scheme of NFC which eliminates the need for dedicated hardware by embedding data stream into the MI signals of a CPU without affecting the normal function of the device.
- A variety of communication schemes are devised using this system, including one-way, full-duplex and multiple transmitter communication to take full advantage of the functionality of the communication devices.
- We prototype the communication system between a laptop and a smartphone as well as between two laptops. Evaluation results demonstrate the efficacy of *MagneComm*.

The rest of this paper is organized as follows: In Sec. 2, we introduce the working principle of the magnetometer and CPU. In Sec. 3, we outline the characteristics of the MI signals generated by CPUs. In Sec. 4, we present the proposed transmission and reception protocols. The prototypes on smartphones and laptops are described in Sec. 5 and evaluations are described in Sec. 6. Future implementations of the proposed system are outlined in Sec. 7. Conclusions are drawn in Sec. 9.

## 2 BACKGROUND

In this section, we outline the working principle of magnetometers and the emission of Magnetic Induction (MI) signals from laptops. These are the fundamental issues related to the design of *MagneComm*.

### 2.1 Magnetometer

A magnetometer is an instrument that measures the magnetization of materials or the strength and direction of the magnetic field at a point in space. The most common magnetic sensors are Hall effect sensors and fluxgate sensors. Hall effect sensors are small and cheap while the sensitivity is low ( $\leq 5mV/mT$ ). They are commonly employed with the gyroscopes and accelerometers used for motion tracking in mobile devices. As illustrated in Fig. 2(a), the voltage develops in a direction transverse to the current flow in p-type semiconductor in a magnetic field owing to Lorentz Force [16]. Hall effect magnetometers utilize the varying output voltage as the indicator to the magnetic field.

Fluxgate magnetometers provide greater sensitivity than Hall effect sensors. They are commonly used to measure DC or high-frequency magnetic field vectors. A fluxgate sensor employs a saturable inductor to sense the field produced by an external current. As shown in Fig. 2(b), a fluxgate magnetic sensor comprises a fluxgate sensor (sensing coil) with sensor conditioning and a compensation coil to internally close the control loop. The fluxgate sensor is repeatedly driven in and out of saturation, thereby enabling hysteresis-free operation with a high degree of accuracy. The internal compensation coil ensures stable gain and high linearity.

In this study, in addition to using built-in Hall effect magnetometers in mobile devices, we also employ a high-performance

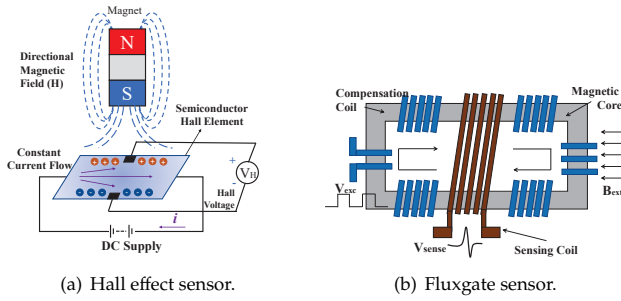


Figure 2: The working principle of two types of magnetometers.

fluxgate sensor, DRV425 from TI [7], to understand the impact of various magnetometers. The output analog signals from DRV425 are sampled by an ADC chip (ADC7606) controlled through STM32F107 Microcontroller Unit. The sampling rate of the ADC is set to 10KHz with 12-bit output resolution (up to  $0.15nT$  per bit). Although higher sampling rates (up to 50KHz) are possible, Magnetic Induction signals from the CPU presents little between 10KHz and 50KHz so a higher sampling rate would only increase the burden of data analysis without providing any benefit.

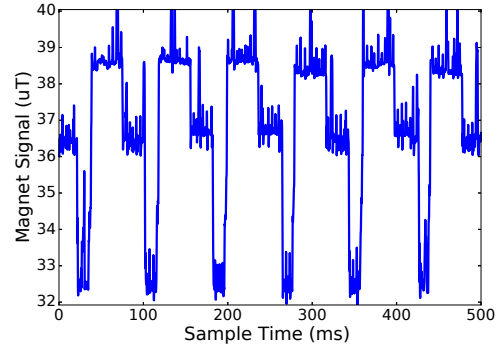
## 2.2 Magnetic Induction from Laptops

A laptop is a complex device with numerous electronic units, such as a CPU, GPU, electronic fan, speaker, hard disk, and battery. Theoretically, any of these units could be used to generate Magnetic Induction signals. By carefully controlling the working pattern of these units, we can embed a data stream in the generated MI signals. For example, the normal working power of a CPU ranges from 20 to 90W. As shown in Fig. 3(a), the strength of Magnetic Induction signals can be adjusted by controlling the usage of the CPU. In addition, electronic fans consume around 3W power. Fig. 3(b) presents MI signals generated by a computer fan in the form of sine waves. Controlling the rotation speed of the fan to vary the phases and frequencies of these sine waves makes it possible to embed information in the MI signals.

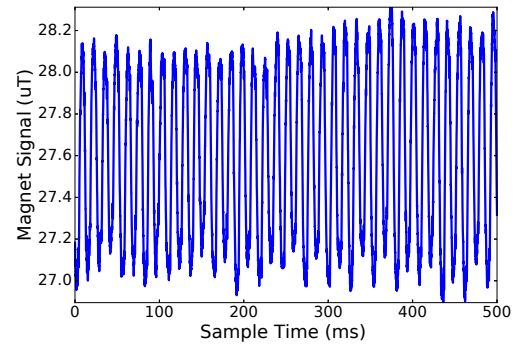
Despite the multiple choices, we focus primarily on the Magnetic Induction signals generated by CPUs in this work. One advantage of using CPUs is that CPU usage can be easily controlled using loop and *sleep* commands, which are available for most programming languages and operating systems. In contrast, for example, controlling the fan may require specific drivers or APIs and is only supported by a few programming languages. Furthermore, it is easier to monitor CPU usage in real-time in order to estimate channel conditions. Finally, the multiple cores in a CPU can be used to design a multiple-transmitter communication protocol. The details of the protocols are discussed in Section 4.

## 3 MAGNETIC INDUCTION FROM CPU

The precise control over CPUs and emitted Magnetic Induction (MI) signals is the key to realize MagneComm. In this section,



(a) CPU.



(b) Fan.

Figure 3: Magnetic Induction signals emitted from CPU and fan.

we investigate the characteristics of the MI signals from CPUs and explore the design space of modulating data bits.

### 3.1 Characteristics

MI signals generated from a CPU are affected by many factors.

**Multi-core CPU:** multi-core CPUs (*i.e.*, CPUs with two or more independent processing units, called “cores”) are common in recent mobile devices. Multiple cores make it possible to run multiple instructions in parallel. Unless otherwise specified in the program or OS, a program with multiple threads may attempt to use all of the cores at once. The fact that each core emits its own MI signals means that the MI signals from a CPU is actual the superposition of all of the cores.

**CPU working status:** different instructions can lead to different patterns in the MI signals, which can be identified by magnetometers with a high sampling rate ( $> 1.7 MHz$ ) [8]. The sampling rate of the magnetometers used in most mobile devices ranges from 10 to 200 Hz. Based on experiment results, this type of magnetometer is able to determine whether a CPU is working or idle, but little else. As shown in Fig. 4, we run a program including four instructions: addition (+), subtraction (-), multiplication (\*), division (/), and then a command for *sleep*. Omitting the glitch signal leaves only two levels of

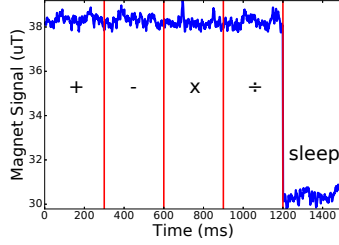


Figure 4: Emitted MI signals while CPU executing various instructions.

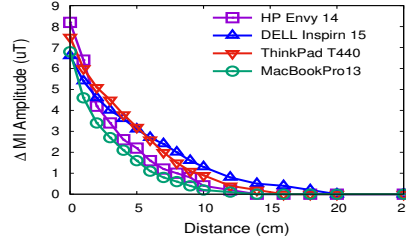


Figure 5: The amplitude change of MI signals of one CPU core at different distances.

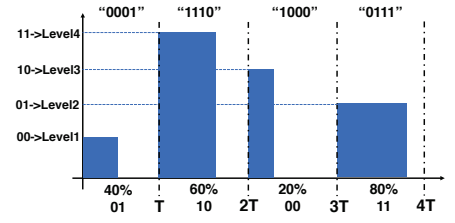


Figure 6: Example of PWAM data symbols.

magnitude in the MI signals, corresponding to the status of the machine (working and idle).

**Distance:** the magnitude of the MI signal is inversely proportional to the cube of the distance traveled. Furthermore, the material with which the case of the mobile device is constructed may also affect the magnitude, due to the shielding effect. Fig. 5 shows the changes in the magnitude of MI signals over distance, as measured using various types of laptops. At each distance, we measure MI signals when the CPU is in working and idle states, and calculate the magnitude difference between two states. We can see that at distances exceeding 10 cm, the magnitude change becomes too small to be distinguished by DRV425 magnetometer with the sensitivity of 0.16 uT.

### 3.2 Controlling Magnetic Induction Signals

In the following, we examine the methods used to control Magnetic Induction and modulate data.

**Modulation:** regular magnetometers can only measure the working and idle status of a CPU core; therefore, one intuitive way to embed data is to use On-Off Keying. That is, we switch a CPU core between idle and working to represent 0 and 1, respectively. For a 200Hz magnetometer, switching CPU status every 5ms would enable a data transmission rate of 200bps. However, in most practical situations, it is difficult to control the CPU in this manner. Furthermore, On-Off keying is subject to noise generated by background programs.

We therefore selected Pulse Width and Amplitude Modulation (PWAM) which combines the Pulse Width Modulation (PWM) and Pulse Amplitude Modulation (PAM) to modulate data. Specifically, each data symbol has period  $T$  and is presented using the proportion of CPU working time during that period. A data symbol consists of  $M + N$  data bits, where  $M$  bits are translated to a set of pre-defined  $2^M$  levels of amplitude of CPU magnetic induction signals (PAM),  $N$  bits are translated to a set of pre-defined  $2^N$  levels of CPU working percentage (PWM). Take Fig. 6 as an example, each data symbol is 30ms long and consists of 4 bits. The amplitude of each symbol could be 1, 4, 3, 2 which represents data bits: 00, 11, 10 and 01. The CPU working percentage of each symbol could be 40%, 60%, 20%, 80% which represents bits: 01, 10, 01 and 11, respectively. We can adjust  $T$ ,  $M$  and  $N$  according to the current channel condition as well as how precise we can control a CPU core.

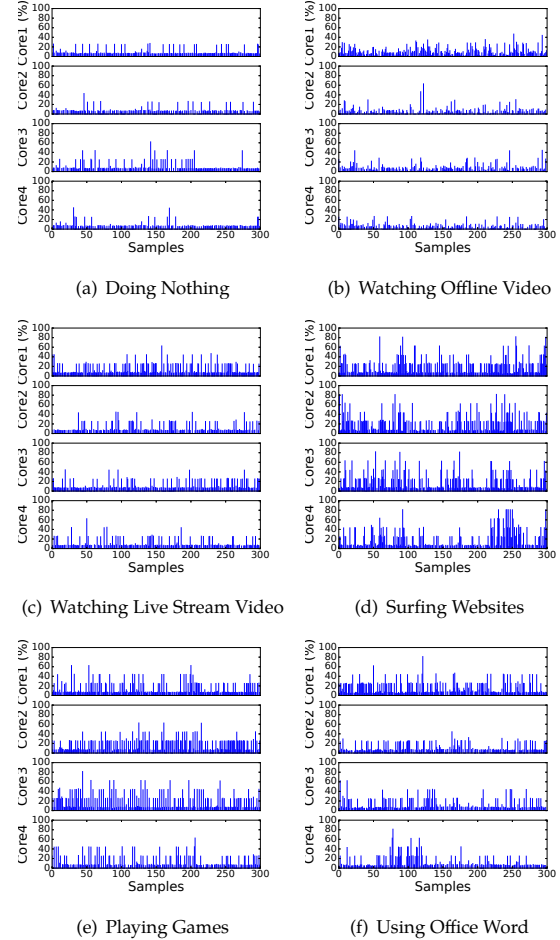


Figure 7: CPU usage of each core recorded every 50ms under various conditions.

**Multiple cores:** modern OSes optimize the scheduling of tasks specifically for multi-core CPUs to ensure efficiency in the execution of commands. The OS maintains queues of global tasks, which can be assigned to any core with free resources. In controlling specific CPU cores to generate a desired magnetic signal, processor affinity [26] can be used to bind a given process to a specific CPU core. As shown in Fig. 3(a), multiple cores can be used to generate the same PWAM symbols in order to increase transmission range, or generate different PWAM symbols for parallel communication. Most operating

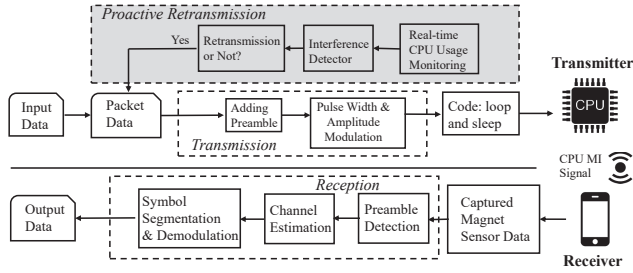


Figure 8: MagneComm operation flow.

systems feature processor affinity. In our prototype, we implemented it in Windows 7, 8, 10, Ubuntu14, MacOS X, and Android 6 and 7.

### 3.3 Noise from Running Programs

It is inevitable that the CPU will be used by the user and/or the OS during the transmission of data. CPU usage from other programs introduces noise to the signals used for communication. We seek to characterize this noise by collecting traces of MI signals while a user performs various activities, including watching offline videos of various resolutions and various video codecs, watching online streaming content, surfing websites, playing games, as well as doing nothing. Fig. 7 shows the corresponding CPU usage on each core. The CPU usage patterns vary little while watching videos and streaming, regardless of the resolution and codec. Thus, this data has been omitted due to space limitations. It is observed that when the computer is not used, the OS continues accessing the CPU for brief periods in the processing of background apps. This indicates that a mechanism is required for the detection of packet corruption and the retransmission of data due to the interference. We also observed that watching videos and streaming only occasionally increase the CPU usage, whereas surfing websites and playing games greatly affect CPU usage. Nonetheless, even for CPU intensive operations, there are numerous intervals of low CPU usage, which could be used for communication.

## 4 TRANSMISSION AND RECEPTION

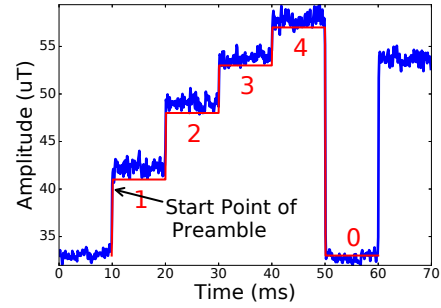
### 4.1 System Overview

MagneComm is designed using the off-the-shelf laptops and smartphones. Fig. 8 illustrates the system architecture which comprises of two parts: a sender (e.g., a laptop’s CPU) and a receiver (e.g., a smartphone’s magnetometer). The sender embeds data with the Magnetic Induction (MI) signals generated by CPU in the laptop. The magnetometer on the phone captures the MI signals and decodes it to extract the transmitted data. The details of each step are described in this section.

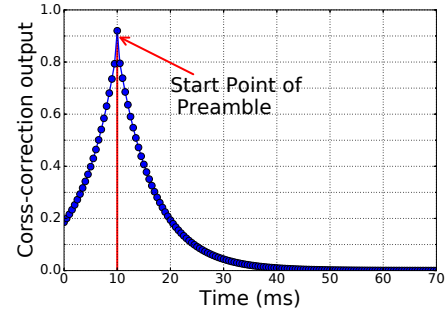
### 4.2 Transmitter Design

MI signals can be generated by controlling the working or idle status of the CPU. In this section, we demonstrate the modulation of data bits while enabling the reliable transmission in the presence of noise caused by other background programs.

**4.2.1 Preamble.** Preamble is used for two purposes. One is to synchronize the sender and the receiver. An unique MI pattern



(a) Preamble Design.



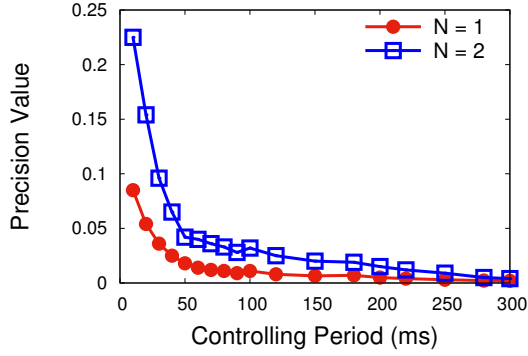
(b) Corss Correlation.

Figure 9: Preamble design and detection.

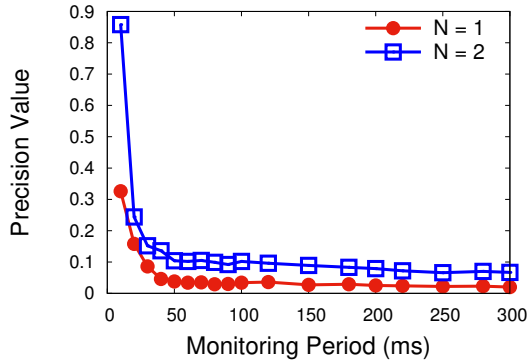
is introduced as the preamble at the beginning of each data frame, thereby allowing the receiver to use cross-correlation to identify the start time of each transmission. The other purpose is to enable the receiver to estimate channel conditions. Because the amplitude of MI signals varies when a different number of CPU cores are being used as well as under different channel conditions. The receiver must be aware of different amplitude values of a PWAM symbol in order to decode it. As shown in Fig. 9, the preamble is designed as a sequence of [1, 2, 3, 4, 0] using four CPU cores, whose communication parameter  $M$  is set as 2. We evaluate the effectiveness of our preamble in Sec. 6.1.

**4.2.2 Modulation.** We opted for PWAM for the modulation of data bits due to its effectiveness and robustness to noise over On-Off Keying. The choice of  $T$ ,  $M$  and  $N$  depends on the precision of controlling and the precision of CPU monitoring.

**Single CPU core control precision:** Fig. 10(a) shows the single CPU core control precision under various  $T$  and  $N$ . The control precision is defined as:  $Prec_{control} = \frac{|U_{real} - U_{desired}|}{[1/(2^N - 1)]}$ , where  $U_{desired}$  is the desired CPU core usage,  $U_{real}$  is the actual CPU core usage generated, and  $1/(2^N - 1)$  is the interval between  $2^N$  levels (e.g., when  $N = 2$ , the interval between 4 levels of CPU core usage is 33%). The closer the value of  $Prec_{control}$  is to 0, the more precisely we can control the CPU cores. And from the Fig. 10(a) we can see that the smaller  $T$  and larger  $N$  reduces CPU controlling precision. The minimal symbol length  $T$  we can choose is 10ms with  $N = 1$  bit per symbol.



(a) CPU Controlling Error.



(b) CPU Monitoring Error.

Figure 10: The precision of CPU control and monitor

**Single CPU core monitor precision:** the transmitter must continuously monitor CPU usage ensure that packets are transmitted correctly. Thus, the precision with which the CPU core usage is monitored also limits the selection of  $T$  and  $N$ . We use MI measurements as a proxy for CPU usage and define monitoring precision in a similar manner:  $Prec_{monitor} = \frac{|U_{sensor} - U_{monitor}|}{[1/(2^N - 1)]}$ , where  $U_{sensor}$  is the CPU core usage estimated using measured MI signal by sensor, and  $U_{monitor}$  is the monitored CPU core usage by OS itself. The results are shown in Fig. 10(b). We can see that the minimal symbol length can be correctly monitored is  $20ms$ . So after combining the limitation of CPU controlling and monitoring, we will select  $T = 20ms, N = 2$  as our fastest transmission rate to modulate the information data bits.

**4.2.3 Proactive Retransmission.** In the scenarios where only the receiver has the magnetometer, the transmitter is not able to get acknowledgement from the receiver to check if a packet is successfully transmitted. Therefore, a corruption detection mechanism on transmitter is important to enable one-way communication in such scenarios. Fortunately, due to the near-field communication property, the major noise is actually generated by background programs. By continuously monitoring the CPU usage on all cores, the transmitter can know if a packet is corrupted due to the noise. Algorithm 1 shows our Proactive Retransmission mechanism.

Algorithm 1 Proactive retransmission on transmitter.

```

function RETRANSMISSION
  while packet  $x$  is sent do
     $SymbolNoise_j \leftarrow \sum_{core\ i} Usage_i$ 
     $ReFlag_x \leftarrow \sum_{symbol\ j} Rule(SymbolNoise[j])$ 
    if  $ReFlag_x \neq 0$  then
      Retransmit(packet  $x$ )
    else
      Transmit(packet  $x + 1$ )
    end if
  end while
end function

```

The transmitter controller monitors the real-time CPU usage on all cores with the same period of PWAM symbols, and after transmitting one packet, it uses the history experience to determine whether existed interfered symbols in the packet. For example, when over two non-transmitter CPU cores have more than 20% usage, the transmitter controller classifies this symbol into the interfered category and  $Rule(SymbolNoise[j])$  would be set as 1. Because we did not employ error correction schemes, the transmitter retransmits the whole packet for any corrupted symbol. The throughput can be further improved if erasure coding [22] or partial packet recovery schemes [14] are introduced.

### 4.3 Receiver Design

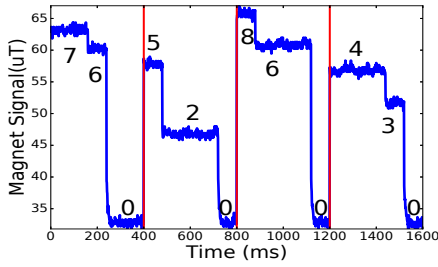
The receiver performs preamble detection for use in synchronization and signal strength estimation. Following the segmentation of symbols, they are demodulated for the extraction of data bits.

**Preamble Detection:** a preamble is used to locate the start of a packet. The receiver applies cross-correlation to locate the preamble pattern accurately, and as mentioned above, channel estimation must be performed prior to the extraction of symbols.

**Symbol Segmentation:** after preamble detection, the data embedded in MI signals can be accurately located. The receiver can easily segment the symbols after preamble with the fixed PWAM length known in advance. And after channel estimation, the receiver determines the amplitude and width information in each symbol, whereupon the original data bits can be recovered.

### 4.4 Enabling Multiple Transmitters

In wireless communication, multiple-antenna systems are generally known to outperform single-antenna system by increasing the transmission bandwidth and effectively countering the multipath and interference. In MagneComm, we employ the same idea and use multi-core CPU to serve as multiple transmitters. For example, in a laptop with the eight-core CPU, one core group consisting of two cores can be treated as the first transmitter, while the other core group consisting of six cores can be treated as the second transmitter. Two core groups can send data concurrently to increase the throughput.



(a) The MI amplitude observed by the receiver.

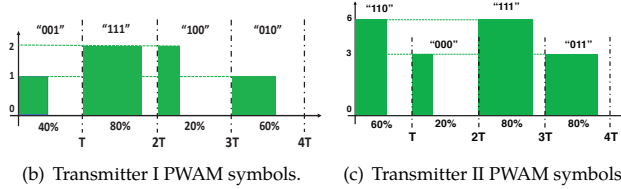


Figure 11: The working principle for multiple transmitters.

In the transmitter, we rely on process affinity for the generation of PWAM symbols using different CPU cores. However, in the receiver, we need a mechanism to distinguish PWAM symbols from different transmitters.

Our solution is based on a simple idea: each transmitter uses different number of CPU cores so the amplitude values of PWAM symbols from different transmitters are different. In the previous example, we allocate two cores to Transmitter one with  $M = 2$ , so it can generate MI signals with amplitudes  $[0, 1, 2]$ ; we allocate six cores to Transmitter two with  $M = 2$ , so it generates  $[0, 3, 6]$  amplitudes. And the superposition of amplitude values are shown in Table. 1. The mixed MI amplitude corresponds to only one pair  $\langle Tx_1 \text{ signal}, Tx_2 \text{ signal} \rangle$ . So the receiver can easily to separate the mixed signals into two signals from Table. 1. Fig. 11 shows a two-transmitter example. When two transmitters are transmitting data bits simultaneously, the first transmitter uses two CPU cores to generate PWAM symbols, with the parameters are:  $T = 300ms$ ,  $M = 1$  and  $N = 2$ , and the second transmitter uses six CPU cores with the same parameters. When the receiver receive PWAM symbol, it detects the amplitude level of each period using the preamble signal as reference, and in this condition the preamble is designed as  $[1, 2, 3, 4, 5, 6, 7, 8, 0]$ . After obtaining the amplitude levels of each symbol, the receiver checks Table. 1 and rebuilds  $Tx_1$  and  $Tx_2$  signals to extract data bits separately.

Table 1: MI amplitudes observed by receivers when two transmitters are transmitting concurrently using different number of cores.

Mixed MI Signal	0	1	2	3	4	5	6	7	8
Tx 1 MI Signal	0	1	2	0	1	2	0	1	2
Tx 2 MI Signal	0	0	0	3	3	3	6	6	6

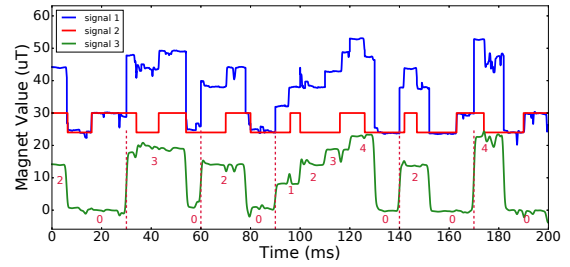


Figure 12: The cancellation principle of full-duplex communication: signal 1 plotted in blue represents the mixed MI signals, signal 2 in red represents the estimated MI signals generated by itself, and signal 3 in green represents the targeted MI signals after cancellation

## 4.5 Enabling Full-Duplex Communication

Full-duplex communication can be achieved when both mobile devices are equipped with magnetometers (*i.e.*, communication between two mobile phones.) The challenge of enabling full-duplex communication is that, when a mobile device is transmitting and receiving data at the same time, the received PWAM symbol is a linear combination of its own transmitted PWAM symbol and targeted PWAM symbol to decode. Fortunately, since the device knows what it is transmitting and has ability to estimate the amplitude of its own PWAM symbol, the device can subtract the transmitted PWAM symbol from the received one and recover the the targeted PWAM symbol. Fig. 12 shows an example to perform full-duplex communication. Considering that the magnetometers equipped on the smartphones are not sensitive enough to capture the other smartphone CPU's MI signals, we use two laptops both equipped with DRV425 magnet sensors to verify the feasibility of our full-duplex design. Specifically, one laptop sets the transmission parameters to:  $T = 30ms$ ,  $M = 0$ ,  $N = 2$ , while the other sets it to:  $T = 30ms$ ,  $M = 2$ ,  $N = 2$ .

## 5 SYSTEM PROTOTYPE

Two sets of prototypes are implemented to evaluate MagneComm.

**Prototype I: Laptop and Phone.** The first prototype employs transmitters on laptops running Windows, Ubuntu, or MacOS X, while the receiver is an Android phone. Laptops are equipped with Intel Core CPU (4 or 8 cores). The Android phone is a Huawei Nexus 6P equipped with a Hall effect magnetometer operating at a sampling rate of 50 Hz. In this prototype, we implement one-way communication with multiple-transmitter enabled. All experiments in Section 6 are repeated using all laptops.

**Prototype II: Laptops with Magnetometers.** The second prototype employs transmitters and receivers on two laptops with external magnetometers (DRV425) attached. In this system, we used the same set of laptops that were used in the first prototype. The magnetometer is a fluxgate sensor with sampling rate of 200 KHz. This prototype involves full-duplex communication with multiple-transmitter enabled.

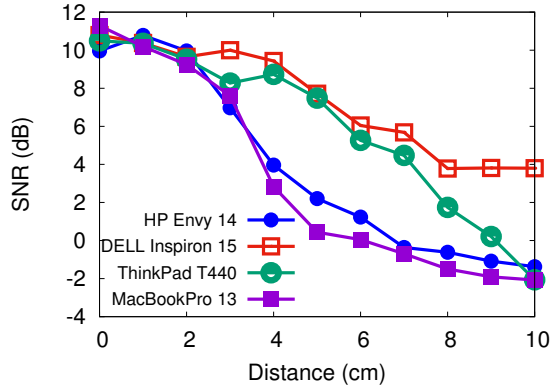


Figure 13: SNR vs. distance using different models of laptops.

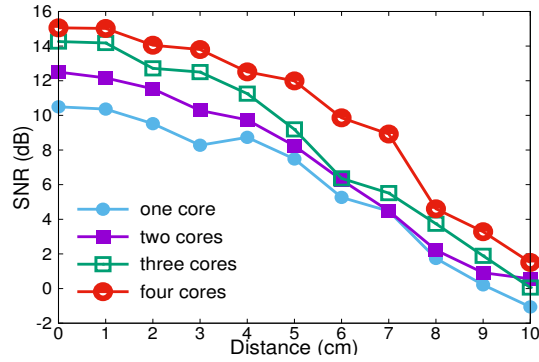


Figure 14: SNR vs. number of working CPU cores.

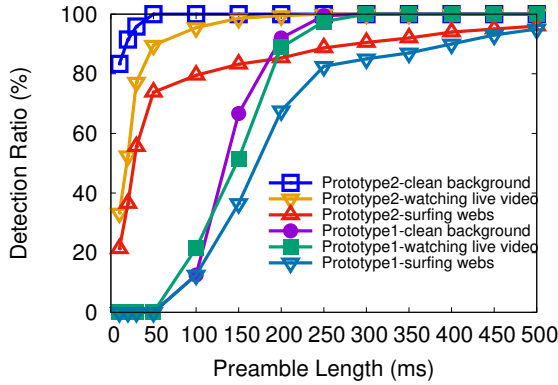


Figure 15: Preamble detection accuracy under various preamble lengths with  $M = 2$ .

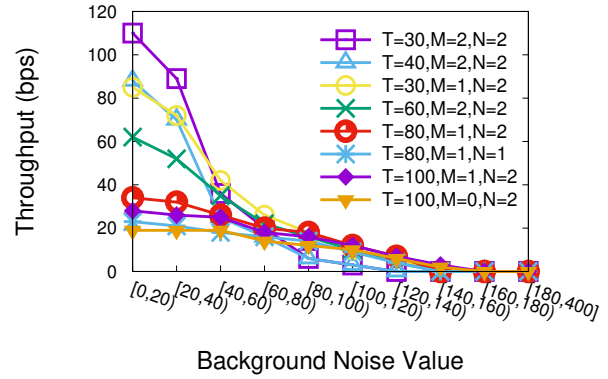


Figure 16: Throughput vs. levels of noise under various symbol length  $T$ .

## 6 EVALUATION

### 6.1 Micro Benchmark

**Communication Distance** : we first use Prototype II where two laptops equipped with external magnetometers to examine the valid communication ranges. Fig. 13 shows the SNR under various transmission distances using four different laptops. We can observe that SNR is similar for all laptops when distance is shorter than 3 *cm*. SNR for HP Envy 14 and MacBookPro 13 drops quickly after 3 *cm* while that from DELL Inspiron 15 remains high at 10 *cm*.

We can boost the transmission distance by utilizing multiple CPU cores. As shown in Fig. 14, the more CPUs used, the higher SNR we can get. At the distance of 5 *cm*, increasing the number of CPU cores from 1 to 4 increases SNR by 4 *dB*.

**Device Orientation** : to verify the impact of the device orientation to the communication, we change the angles of the receiver by 15°, 30°, 45°, 60°, and 75° while being placed at the same location. The results show that the device orientation has no influence to the observed MI signals. It's because that there are three orthogonal magnet sensors on a magnetometer and we calculate the square root of sum of the magnetism from

three dimensions so it becomes independent to the device orientation.

**Preamble Length** : a longer preamble makes it easier to control CPU cores to generate the desired preamble pattern and is more robust against the noise. However, the longer preamble also results in the larger communication overhead. To obtain the best preamble length for MagneComm while background noise exists, we vary the preamble length and use Prototype I and II to test the ratio where preambles are correctly detected. Fig. 15 shows the results. We can see that 80% – 100% of preambles can be correctly detected when the length is 300 *ms* in Prototype I, and 50 *ms* in Prototype II.

**PWAM parameters** : In Sec. 4.2 we show that the symbol length  $T$  needs to be 20 *ms* or longer in order to precisely control and monitor the CPU usage. Nonetheless, channel condition also has impact to the selection of  $T$ . A shorter symbol period implies a higher data rate while it can also be more fragile to the noise. To find the best parameters for PWAM modulation, we vary  $T$ ,  $M$ ,  $N$  under different levels of noise using Prototype II. The level of noise is defined as the CPU usage caused by background programs. Each experiment lasts for 10 minutes. The corresponding throughputs are shown in Fig. 16.

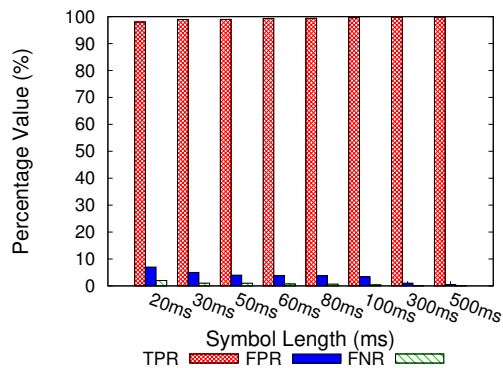


Figure 17: Corruption detection performance on the transmitter.

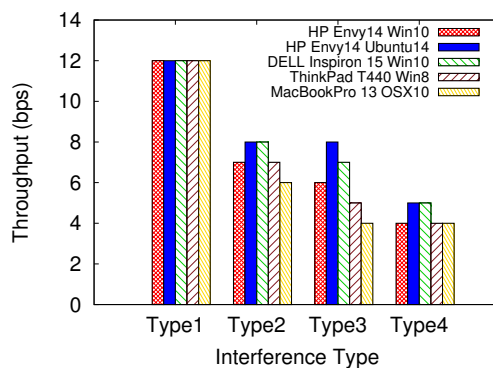
We can observe that when the noise is small, using shorter symbol period  $T$  yields a larger throughput, as expected. When the noise value is 40% or larger, lower data rates with larger  $T$  start to out-perform because they can tolerate more noise. The results suggest that we can design a rate adaptation and use a look-up table to decide the best data rate for the current channel condition. We focus on the basic design of MagneComm in this work and leave the rate adaptation as the future work.

**Corruption Detection from Transmitter:** the success of one-way communication relies on that if a transmitter can correctly detect and retransmit corrupted packets. We transmit PWM symbols with  $T$  varying from 20 to 500 ms and  $N = 2$  bits for 10 minutes in Prototype II, and evaluate the corruption detection accuracy.

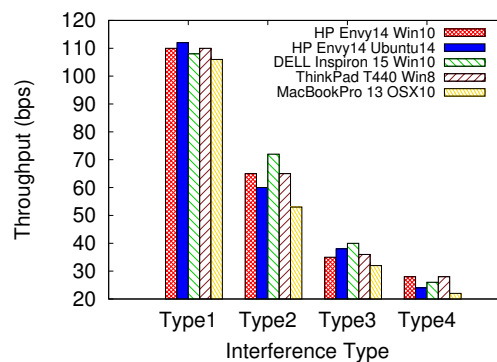
The results are shown in Fig. 17. True Positive Rate (TPR) represents the number of symbols which are actually corrupted and are detected as corrupted to the number of actually corrupted symbol. False Positive Rate (FPR) represents the number of symbols which are correct but are detected as corrupted to the number of actually correct symbol. False Negative Rate (FNR) represents the number of symbols which are actually corrupted but are detected as correct symbol to the number of actually corrupted symbols. We can see that TPR is 99.6% or higher while FNR is 0.5% or lower when the symbol length is 30 ms or longer, which indicates that our corruption detection algorithm on transmitter can correctly detect corrupted symbols. Therefore, in our following experiments, we select the 30 ms as the fastest transmission rate instead of 20 ms.

## 6.2 One-Way Communication Performance

We evaluate the one-way communication performance using two prototypes described in Sec. 5. In Prototype I where a laptop is the transmitter and the mobile phone (Nexus 6P) is the receiver, PWAM symbol length is set to 200ms and each symbol contains 4 bits ( $M = N = 2$ ). In Prototype II where one laptop acts as the transmitter and the other laptop acts as the receiver, the symbol length is set to 30 ms and each symbol contains 4 bits ( $M = N = 2$ ). Each experiment lasts for 10 minutes and is repeated for 10 times. The average throughput is reported.



(a) Prototype I: throughput vs. scenarios.

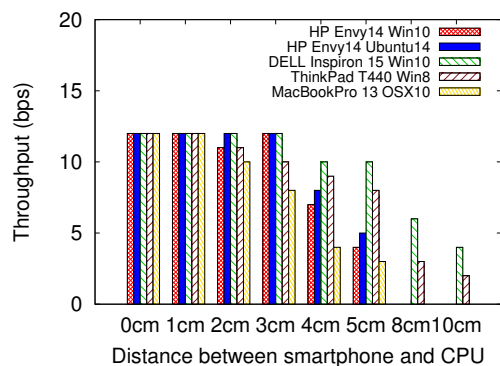


(b) Prototype II: throughput vs. scenarios.

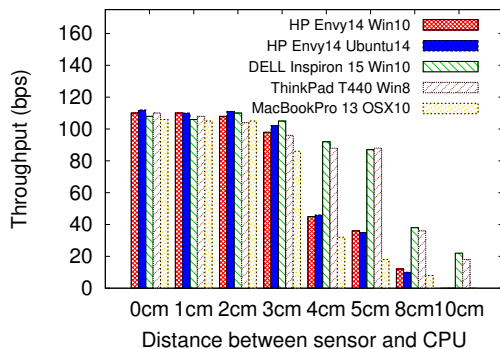
Figure 18: Throughput under various scenarios for one-way communication. In Prototype I,  $T = 300ms$ ,  $M = 2$ ,  $N = 2$ . In Prototype II,  $T = 30ms$ ,  $M = 2$ ,  $N = 2$ . All laptops use 4 CPU cores for transmission. Scenario type 1 to 4 correspond to that the user is doing nothing, watching live video, surfing websites, and playing games, respectively.

Fig. 18(b) and Fig. 18(a) first show how MagneComm perform while using different laptops as transmitters. The 4 laptops have various OSes (Win8, Win10, Ubuntu14 and MacOSX10) and CPU models (Intel i5 with 4 cores and i7 with 8 cores). When there is no other program running, MagneComm achieves 12 bps in Prototype I and 110 bps in Prototype II. While the noise is present, the throughput decreases. For example, while the user is surfing websites, the throughputs drop to 7 bps and 60 bps, respectively.

Fig. 19(b) and Fig. 19(a) show the throughput under various transmission ranges when there is no background noise. We make several observations. First, the throughput remains high for all types of transmitters when the range is 3 cm. Second, due to the SNR drops over distance, the valid communication for all transmitters is 5 cm and 8 cm for Prototype I and II, respectively. Finally, after 3 cm, the throughput of different transmitters varies significantly. More specifically, the throughput of ThinkPad T440 and DELL Inspiron 15 only drops by 26% at the distance of 5 cm while that of other laptops drops by more than 60% at the same distance.



(a) Prototype I: throughput vs. distances.



(b) Prototype II: throughput vs. distances.

Figure 19: Throughput under various distances for one-way communication. In Prototype I,  $T = 300ms$ ,  $M = 2$ ,  $N = 2$ . In Prototype II,  $T = 30ms$ ,  $M = 2$ ,  $N = 2$ . All laptops use 4 CPU cores for transmission.

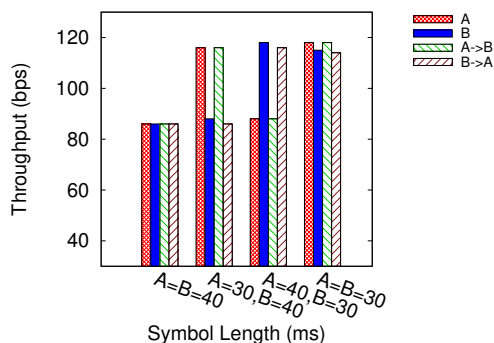


Figure 20: Full-duplex Performance Analysis. A->B means laptop A transmit data to B. Similar definition is also applied to B->A.

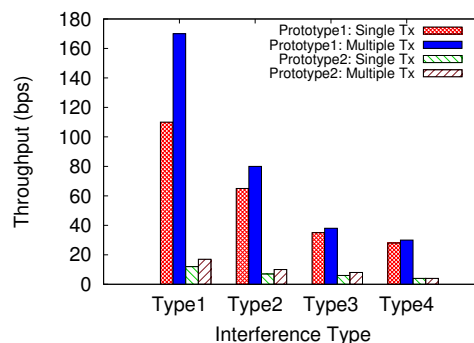


Figure 21: Multiple Transmitters performance analysis. Scenario type 1 to 4 correspond to that when the user is doing nothing, watching live video, surfing websites, and playing games, respectively.

In addition to Prototype I and II, we also implement another prototype where an Android phone acts as the transmitter and a laptop with an external magnetometer acts as the receiver. The Android phone is a Huawei Nexus 6P equipped with a Octa-core CPU, and the laptop is equipped with an external magnetometer. One-way communication is installed in this prototype with the throughput of 95 bps and maximal communication range of 4 cm. We exclude the details of evaluation due to the page limit.

### 6.3 Full-Duplex Communication Performance

We evaluate the full-duplex communication performance using Prototype II where two laptops are equipped with magnetometers and transmit data at the same time. Two laptops' CPUs are 3 cm away from each other. In Fig. 20, we show the throughput of two transmission directions in full-duplex communication and the throughput in one-way communication. Note that  $A$  and  $B$  represents the throughput in one-way communication where  $A$  and  $B$  acts as the receiver, respectively.  $A \rightarrow B$  represents the throughput in full-duplex communication where  $A$  transmits data to  $B$ . We can see that when the

total throughput in full-duplex communication (*i.e.*,  $A \rightarrow B + A \leftarrow B$ ) is 195.5% of that in one-way communication. It implies that our cancellation mechanism works effectively so the total throughput is almost doubled.

### 6.4 Multiple Transmitters Performance

We evaluate the performance of Multiple Transmitters protocol using both prototypes under one-way communication. Fig. 21 shows the results. By increasing the number of tx antennas (*i.e.*, the number of cores) from 1 to 2, the throughput is increased by 141.6% and 154.5% in Prototype I and II under the clean background, respectively. In noisy scenarios, the performance of the Multiple Transmitters protocol decreases because using multiple cores increases the risk of being interfered by the noise.

### 6.5 Energy Consumption

We measure the power consumption of MagneComm when HP Envy 14-j 104TX with Intel Core i7 6700HQ CPU acts as the transmitter and DRV425 magnetometer acts as the receiver.

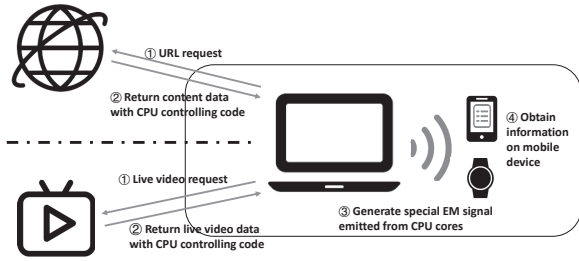


Figure 22: *MagneCode* and Expanded Screen.

The transmitter uses one core to generate one-way traffic for 1.5 hours. The average power consumption is reported in the Table. 2. For comparison, we also estimated the energy consumption of the Bluetooth 4.0 (BLE) [1], Wi-Fi (IEEE 802.11ac) [24], NFC (ISO-13157) [19], and Pulse [13]. Although the energy consumption of *MagneComm* is higher than other protocols, its capability of providing additional bandwidth using existing hardware is still valuable. Moreover, there are many techniques which can potentially reduce the power consumption of *MagneComm*, which includes using finer granularity of CPU duty cycle, reducing the maximal CPU usage level, applying error correction to improve the throughput, and etc. We leave it as our future work.

Table 2: Energy consumption of various communication protocols.

Protocols	Throughput	Watt	J/bit
BLE	0.27Mbps	0.5W	$1.9 \times 10^{-6}$
802.11ac	350Mbps	2.4W	$6.8 \times 10^{-9}$
NFC	424kbps	0.6W	$1.4 \times 10^{-6}$
Pulse	44bps	$8.3 \times 10^{-4}W$	$1.9 \times 10^{-5}$
<b>MagneComm</b>	110bps	5.2W	$4.8 \times 10^{-2}$

## 7 DISCUSSION AND APPLICATIONS

In this section, we discuss a number of potential applications for *MagneComm*.

### 7.1 MagneCode & Expanded Screen

When using a laptop or mobile device, it is common nowadays to obtain information using a QRCode; however, this is not always possible when using a smaller mobile device, such as a smart watch, because they may not have a camera. Nonetheless, even the smallest devices are equipped with a magnetometer for e-compass functionality.

A magnetometer can be used to extract data embedded in MI signals. Thus, *MagneCode* can serve as an alternative to QRCode when camera is not available. As shown in Fig. 22, when a user wants to use a mobile device to obtain additional information, they first request the URL, which returns the controlling code that allows the laptop to generate *MagneCode*.

Moreover, *MagneCode* can be used to add background information, such as player statistics or advertisements, to the video content being viewed by the user and shown on an expanded screen without interfering with the original content.

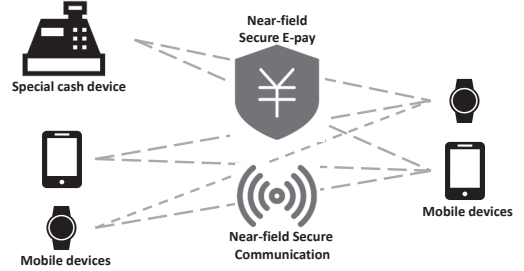


Figure 23: *MagnePay*.

### 7.2 MagnePay

NFC and RFID are mainstays of the near-field wireless communication systems used for e-commerce. Both of these technologies allow convenient e-payment; however, not all mobile devices are equipped with NFC. Furthermore, most payment cards are suitable for only one payment scenario; that is, unified e-payment systems have yet to be implemented. *MagneComm* technology could be used to fill this vacancy, based on the fact that magnetometers are used in nearly all mobile devices. When NFC and RFID becomes increasingly available, *MagneComm* can still complement them by providing extra bandwidth or empowering those old mobile devices.

Therefore, we propose a unified, safe, and convenient e-payment system called *MagnePay*. As shown in Fig. 23, we develop a device capable of generating an MI signals specific for businesses. The device can be used to embed business-related information within an MI signals, which can be accessed by customers on a mobile device (smartphone or smartwatch). This could also be used to make payments for friends, wherein one smartphone is used to generate the special MI signals and acts as a transmitter, while the other smartphone acts as a receiver, without the need for any special device.

## 8 RELATED WORK

Near-field wireless communication has attracted considerable attention due to the richness of the potential applications. Numerous techniques have been developed using a variety of media to enable the communications.

**Visual:** Visible light communication (VLC) provides over bandwidth  $10K \times$  greater than that of the common radio spectra. Due to its directionality and containment, VLC is also a good candidate for near-field communication [17]. In [21], the researchers proposed a novel near-field communication system for smartphones based on visible light, wherein data is encoded using different colors. Unfortunately, VLC generates redundant light pollution and its line of sight characteristics means that it cannot pass through obstacles. [25] presented a method by which to use VLC in dark environments; however, the LED drivers currently available are unable to modulate data bits into light pulse, and replacing existing LEDs would be very expensive.

Quick Response Codes (QRCodes) and other 2D barcodes, also belong to visual near-field communication. QRCodes are widely used in advertising and payments. Strata [11] proposed

a layered coding scheme to enable visual communications and improve the scalability of QRcodes. Strata can dynamically adjust the transmission rates corresponding to a diversity of operating conditions, such as camera resolution and frame rates. Unfortunately, camera sensors are still not available on most wearable mobile devices. Moreover, the information embedded in QRcodes is fixed, and does not support streaming.

**Vibration:** Ripple [18, 23] explored the possibility of using physical vibrations as a mode of wireless communication. When implemented on two mobile devices in which the transmitter regulated vibrations and the receiver sensed them using accelerometers, Ripple achieved data transmission rates of 80bps on Android smartphones [23]. Ripple II [18] featured a redesigned receiver and the microphone is used to sense vibrations. Following the application of OFDM to the design of the physical layer, Ripple II achieved a transmission rate of 30Kbps. An ideal application of vibration communication would be in the development of body networks, where human bone could be used to transfer vibration signals. Unfortunately, in other scenarios, noise caused by the vibration limits applicability.

**Audio:** Acoustic communication over speaker-microphone links has also been explored for near-field communication. Dolphin [27] is a real-time acoustic-based dual-channel communication system in which a speaker is used as a transmitter and microphones are used as receivers. Data signals can be embedded within the original audio signal (as with the audio signal of TV shows), without any perceived difference in the original audio signal. This method has achieved data transmission rates of 500bps on smartphones. In [15], a near-ultrasound communication system was developed using the speakers of TVs and the microphone on a smartphone. This system is able to transmit data at 15 bps in a typical TV-watching environment.

**Magnet:** NFC Standards are mature short-range communication technologies based on magnetic induction. These systems rely on near-field coupling (approximately 5cm) without the need for a discovery mechanism. NFC can achieve data rates of up to 424kbps. Pulse [13] is a system that avoids the need for specialized hardware on the receiver. Rather, it uses two solenoids as transmitters (generating a modulated magnetic signal), and the magnetometer on mobile phones are used to decode the magnetic signals. The key advantage of Pulse is its use of a magnetometer, which is common on current smartphones. Nonetheless, Pulse still requires a purpose-built solenoid for use as a transmitter. A number of commercial products based on magnetic communication, such as LibertyLink docker [28] and FreeLinc's Near Field Magnetic Induction [20], have been implemented in situations requiring a secure and reliable communications channel. However, the need for antennas or coils limits their popularity.

MagneComm enables magnetic communication using components that are already available in almost all mobile devices. Thus, implementation requires only software for the transmitter and receiver. We have also developed a one-way communication protocol for scenarios in which transmitters are not equipped with a magnetometer. MagneComm also works

in full-duplex mode while making full use of the transmitter hardware.

**Other Magnet Application:** One of the most common applications for magnet sensing is localization. In [6, 12], features of the Earth's magnetic field were used to implement indoor navigation systems. [12] proposed a unique cloud platform that runs disruptive geomagnetic positioning in its core to accurately pinpoint locations within a building using the magnetometer in smartphones. [6] demonstrated the feasibility of using an array of e-compasses to measure disturbances in the Earth's magnetic field caused by structural steel elements for use in indoor localization applications.

Devices with currents inside their electronic units produce magnetic field is also a well-known fact and explored for many applications. [9, 10, 29, 30] utilize magnetometers to track Electromagnetic changes emitted from different CPU operations and infer private information. Finexus [4] and uTrack [3] proposed to use the change in magnetic field to track motions of multiple fingertips. DOSE [5] used time-varying electromagnetic interference to monitor the operating states of appliance and infer human activities. uTouch [2] enabled touch interaction on a non-touch LCD by sensing electromagnetic interference when a user brings their hand near or touches the LCD's front panel. These applications are different from our work and focus on utilizing magnetic field in security domain or explore the usage for human-computer interaction.

## 9 CONCLUSION

In this paper, we present a novel approach for near-field communication using Magnetic Induction signals. The proposed system, called MagneComm, is implemented on laptops and smartphones. Systematic analysis of the characteristics of MI signals emitted from the CPU opens the door to using independent CPU cores to transmit data. MagneComm can be used for one-way communication with proactive retransmission to ensure the reliability of communication. It can also be used for full-duplex communication as long as the transmitter and receiver are both equipped with a magnetometer and both have the ability to generate an MI signal. The efficacy of this approach is demonstrated in experiments where MagneComm achieves throughput of 110 *bps* over a distance of up to 10 *cm* between devices. Between a laptop computer and smart phone, we achieve throughput of 12 *bps*. MagneComm complements existing near-field communication protocols with dedicated hardware by providing additional bandwidth. In the future, we will focus on boosting data rate with sophisticated data modulation and rate adaptation schemes, as well as developing the wide range of applications to which the MagneComm system could be applied.

## Acknowledgements

We are grateful to our shepherd Swarun Kumar and anonymous reviewers for their constructive feedback. This work was supported by NSFC grant 61572324, Shanghai Talent Development Fund, and Fundamental Research Funds for the Central Universities 2017QNA4017.

## REFERENCES

- [1] Bluetooth Low Energy 2017. Bluetooth 4.0 BLE. (2017). [https://en.m.wikipedia.org/wiki/Bluetooth\\_Low\\_Energy](https://en.m.wikipedia.org/wiki/Bluetooth_Low_Energy).
- [2] K. Chen, G. A. Cohn, S. Gupta, and S. N. Patel. 2013. uTouch: Sensing Touch Gestures on Unmodified LCDs. In *Proceedings of the SIGCHI Conference on Human Factors in Computing Systems (CHI '13)*. ACM, New York, NY, USA, 2581–2584. <https://doi.org/10.1145/2470654.2481356>
- [3] K. Chen, K. Lyons, S. White, and S. Patel. 2013. uTrack: 3D Input Using Two Magnetic Sensors. In *Proceedings of the 26th Annual ACM Symposium on User Interface Software and Technology (UIST '13)*. ACM, New York, NY, USA, 237–244. <https://doi.org/10.1145/2501988.2502035>
- [4] K. Chen, S. N. Patel, and S. Keller. 2016. Finexus: Tracking Precise Motions of Multiple Fingertips Using Magnetic Sensing. In *Proceedings of the 2016 CHI Conference on Human Factors in Computing Systems (CHI '16)*. ACM, New York, NY, USA, 1504–1514. <https://doi.org/10.1145/2858036.2858125>
- [5] K. Y. Chen, S. Gupta, E. C. Larson, and S. Patel. 2015. DOSE: Detecting user-driven operating states of electronic devices from a single sensing point. In *2015 IEEE International Conference on Pervasive Computing and Communications (PerCom)*. 46–54. <https://doi.org/10.1109/PERCOM.2015.7146508>
- [6] J. Chung, M. Donahoe, C. Schmandt, I. Kim, P. Razavai, and M. Wiseman. 2011. Indoor Location Sensing Using Geo-magnetism. In *Proceedings of the 9th International Conference on Mobile Systems, Applications, and Services (MobiSys '11)*. ACM, 141–154.
- [7] DRV425 2016. Integrated Fluxgate Magnetic Sensor IC for Open-Loop Applications. (2016). <https://www.ti.com/product/DRV425>.
- [8] D. Genkin, L. Pachmanov, I. Pipman, and E. Tromer. 2015. Stealing Keys from PCs Using a Radio: Cheap Electromagnetic Attacks on Windowed Exponentiation.. In *CHES (Lecture Notes in Computer Science)*, Vol. 9293. Springer, 207–228.
- [9] D. Genkin, I. Pipman, and E. Tromer. 2015. Get your hands off my laptop: physical side-channel key-extraction attacks on PCs - Extended version. *J. Cryptographic Engineering* 5, 2 (2015), 95–112. <http://dblp.uni-trier.de/db/journals/jce/jce5.html#GenkinPT15>
- [10] W. Gu, Z. Yang, L. Shangguan, X. Ji, and Y. Zhao. 2014. ToAuth: Towards Automatic Near Field Authentication for Smartphones. In *2014 IEEE 13th International Conference on Trust, Security and Privacy in Computing and Communications*. 229–236. <https://doi.org/10.1109/TrustCom.2014.34>
- [11] W. Hu, J. Mao, Z. Huang, Y. Xue, J. She, K. Bian, and G. Shen. 2014. Strata: Layered Coding for Scalable Visual Communication. In *Proceedings of the 20th Annual International Conference on Mobile Computing and Networking (MobiCom '14)*. ACM, 79–90.
- [12] IndoorAtlas 2017. IndoorAtlas. (2017). <http://www.indooratlas.com>.
- [13] W. Jiang, D. Ferreira, J. Ylioja, J. Goncalves, and V. Kostakos. 2014. Pulse: Low Bitrate Wireless Magnetic Communication for Smartphones. In *Proceedings of the 2014 ACM International Joint Conference on Pervasive and Ubiquitous Computing (UbiComp '14)*. ACM, 261–265.
- [14] H. Balakrishnan K. Jamieson. 2007. PPR: partial packet recovery for wireless networks. In *ACM SIGCOMM Computer Communication Review*. ACM, 409–429.
- [15] S. Ka, T. H. Kim, J. Y. Ha, S. H. Lim, S. C. Shin, J. W. Choi, C. Kwak, and S. Choi. 2016. Near-ultrasound Communication for TV's 2Nd Screen Services. In *Proceedings of the 22Nd Annual International Conference on Mobile Computing and Networking (MobiCom '16)*. ACM, 42–54.
- [16] Lorentz force 2017. Lorentz force. (2017). [https://en.wikipedia.org/wiki/Lorentz\\_force](https://en.wikipedia.org/wiki/Lorentz_force).
- [17] M. Kavehrad N. Chi, H. Haas and T.D. Little. 2015. Visible light communications: demands factors, benefits and opportunities. In *IEEE Wireless Communications*.
- [18] R.R. Choudhury N. Roy. 2016. Ripple II: Faster Communication through Physical Vibration. In *13th USENIX Symposium on Networked Systems Design and Implementation (NSDI 15)*. USENIX Association.
- [19] NFC ISO 13157 2017. NFC ISO 13157. (2017). [https://en.wikipedia.org/wiki/Near\\_field\\_communication](https://en.wikipedia.org/wiki/Near_field_communication).
- [20] NFMI 2017. NFMI by FreeLinc. (2017). <http://www.freelinc.com/technology>.
- [21] J. Niu, W. Song, C. Liu, L. Shu, and C. Chen. 2014. NECAS: Near field communication system for smartphones based on visible light. In *IEEE Wireless Communications and Networking Conference, WCNC 2014, Istanbul, Turkey, April 6-9, 2014*. 2426–2431.
- [22] Luigi Rizzo. 1997. Effective erasure codes for reliable computer communication protocols. In *ACM SIGCOMM Computer Communication Review*. ACM, 24–36.
- [23] N. Roy, M. Gowda, and R. R. Choudhury. 2015. Ripple: Communicating through Physical Vibration. In *12th USENIX Symposium on Networked Systems Design and Implementation (NSDI 15)*. USENIX Association, Oakland, CA, 265–278.
- [24] P. P. Inamdar S. K. Saha, P. Deshpande. 2015. Power-throughput tradeoffs of 802.11n/ac in smartphones. In *IEEE Conference on Computer Communications (INFOCOM)*. IEEE.
- [25] K. Wright T. Zhao and Z. Xia. 2016. The DarkLight Rises: Visible Light Communication in the Dark. In *In Proc. of MobiCom*.
- [26] TMurgent Technologies. 2003. *White Paper: Processor Affinity*. TMurgent Technologies.
- [27] Q. Wang, K. Ren, M. Zhou, T. Lei, D. Koutsonikolas, and L. Su. 2016. Messages Behind the Sound: Real-time Hidden Acoustic Signal Capture with Smartphones. In *Proceedings of the 22Nd Annual International Conference on Mobile Computing and Networking (MobiCom '16)*. ACM, 29–41.
- [28] Dan Wolfson. 2003. The LibertyLink Docker Wireless Headset. *Computing Unplugged* (December 2003).
- [29] A. Zajic and M. Prvulovic. 2014. Experimental Demonstration of Electromagnetic Information Leakage From Modern Processor-Memory Systems. *IEEE Transactions on Electromagnetic Compatibility* 56, 4 (Aug 2014), 885–893. <https://doi.org/10.1109/TEMC.2014.2300139>
- [30] Z. Zhu, H. Pan, Y. Chen, X. Ji, F. Zhang, and C. You. 2016. MagAttack: Remote App Sensing with Your Phone. In *Proceedings of the 2016 ACM International Joint Conference on Pervasive and Ubiquitous Computing: Adjunct (UbiComp '16)*. ACM, New York, NY, USA, 241–244. <https://doi.org/10.1145/2968219.2971404>